Wiley Analytical Science

Wiley Analytical Science Virtual Conference

November 9-17

For the 3rd time, The Wiley Analytical Science Conference is back!

It's all happening November 9 - 17

The Wiley Analytical Science Virtual Conference will bring together thousands of researchers and practitioners to share current developments in science and industry. Join for exciting presentations from experts in the fields of analytical and bioanalytical chemistry, pharmaceutical research, materials science, lab automation, and related disciplines.

Register to learn about recent developments & applications in:

- Microscopy
- Spectroscopy
- Mass Spectrometry
- Separation Science
- Much more!

Register here

WILEY

ADVANCED MATERIALS
www.advmat.de

Cell-Traction-Triggered On-Demand Electrical Stimulation for Neuron-Like Differentiation

Zhirong Liu, Mingjun Cai, Xiaodi Zhang, Xin Yu, Shu Wang, Xingyi Wan, Zhong Lin Wang, and Linlin Li**

Electromechanical interaction of cells and extracellular matrix are ubiquitous in biological systems. Understanding the fundamentals of this interaction and feedback is critical to design next-generation electroactive tissue engineering scaffold. Herein, based on elaborately modulating the dynamic mechanical forces in cell microenvironment, the design of a smart piezoelectric scaffold with suitable stiffness analogous to that of collagen for on-demand electrical stimulation is reported. Specifically, it generated a piezoelectric potential, namely a piezopotential, to stimulate stem cell differentiation with cell traction as a loop feedback signal, thereby avoiding the unfavorable effect of early electrical stimulation on cell spreading and adhesion. This is the first time to adapt to the dynamic microenvironment of cells and meet the electrical stimulation of cells in different states by a constant scaffold, diminishing the cumbersomeness of inducing material transformation or trigging by an external stimulus. This in situ on-demand electrical stimulation based on cell-traction-mediated piezopotential paves the way for smart scaffolds design and future bioelectronic therapies.

1. Introduction

The cell microenvironment is a key determinant of modulating cell behavior and function in tissue development, physiology, and pathophysiology.[1] The extracellular matrix (ECM) in the cell microenvironment not only acts as structural support for cells but also provides a train of biochemical and biophysical cues to regulate cell behaviors and trigger tissue functions.[2] An in-depth understanding of the evolution of cell microenvironment over time and modeling of this dynamic microenvironment are essential for tissue regeneration. Biomimetic materials with time-modulated properties, that is, 4D biomimetic materials, have drawn increasing attention due to their bionic nature. Triggered by external stimuli (e.g., temperature, light, electricity, and magnetic field), 4D biomimetic materials exhibit specific changes of their own characteristics, such as mechanical property, hydrophobic/hydrophilic property, redox state, and conformation of surface ligands, to build a dynamic cell microenvironment.[3] However, most existing 4D bionic systems need external stimuli, which is inconvenient for patients, and may limit their clinical transformation.

Recently, researchers found that there is a bi-directional interaction between cells and ECM.[4] Specifically, cells do not merely respond passively to biochemical and biophysical signals that are delivered to them.[5] Instead, many cells actively alter their surrounding environment to suit their needs, including soluble factor secretion and matrix deposition, degradation, and reorganization.[6] Among them, the mechanical interaction between cells and substrates has been widely studied, mainly focusing on the regulation of cell adhesion and behavior by stiffness of the substrate, as well as the reorganization of the substrate morphology by cell traction.[7] However, the dynamic interactions between cells and substrates at different stages are rarely studied. Moreover, how this dynamic process directs cells behaviors remains relatively unexplored.

In this work, we fabricated a piezoelectric fibrous network with mechanical stiffness similar to that of collagen and applied this network to elucidate the dynamic mechanical interaction between cells and substrates. Mature focal adhesion (FA) is one of the necessary conditions for cell-substrate bi-directional mechanical perception. Thus, the whole process involves two distinct stages: i) "slippage". Before the formation of mature FAs, cells and substrate do not perceive each other's mechanical behaviors, thereby cell activity causes relative slippage of the cells to the substrate without causing nanofiber deformation (Video S1, Supporting Information); and ii) "traction". After the formation of mature FAs, the intracellular biophysical

Z. Liu, X. Zhang, X. Yu, S. Wang, X. Wan, Z. L. Wang, L. Li
Beijing Institute of Nanoenergy and Nanosystems
Chinese Academy of Sciences
Beijing 101400, P. R. China
E-mail: zhong.wang@mse.gatech.edu; lilinlin@binn.cas.cn
Z. Liu, X. Wan, Z. L. Wang, L. Li
School of Nanoscience and Technology
University of Chinese Academy of Sciences
Beijing 100049, P. R. China
M. Cai
State Key Laboratory of Electroanalytical Chemistry
Changchun Institute of Applied Chemistry
Chinese Academy of Sciences
Changchun, Jilin 130022, P. R. China
Z. L. Wang
School of Materials Science and Engineering
Georgia Institute of Technology
Atlanta, GA 30332-0245, USA
The ORCID identification number(s) for the author(s) of this article can be found under https://doi.org/10.1002/adma.202106317.

DOI: 10.1002/adma.202106317

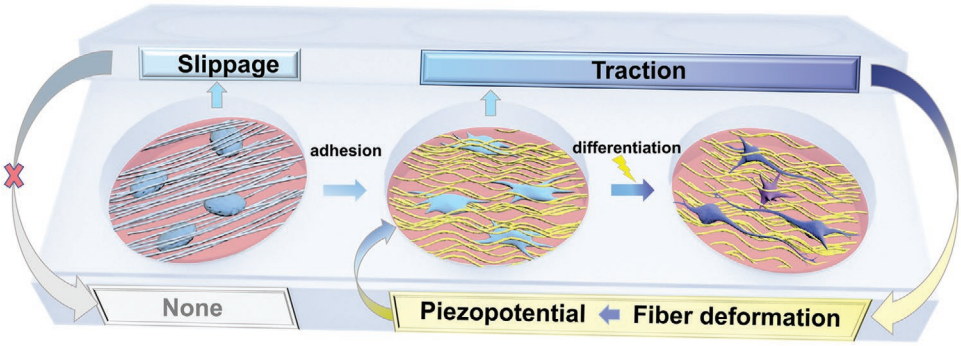

Figure 1. Schematic diagram of the cell-traction-triggered on-demand electrical stimulation for neuron-like differentiation.

signal can be transmitted to exterior via the integrin-mediated force transduction to deform the fibrous network (Video S2, Supporting Information). Based on the mechanical–electrical conversion of the piezoelectric fibrous network and dynamic mechanical interaction between the cells and the cell microenvironment, we established an in situ, wireless, and on-demand electrical stimulation system to stimulate stem cell behavior and differentiation. The system generated piezopotential only when cell differentiation was needed, while no piezopotential in the process of cell spreading and adhesion due to immature FAs (**Figure 1**).

2. Results and Discussion

Electrospinning technology was employed to fabricate poly(vinylidene fluoride) (PVDF) piezoelectric nanofiber scaffold due to their dimensional similarity to native ECM[8] and tunable stiffness. In addition, the high surface area and open interconnected porous structure of the electrospun nanofibers are conducive to nutrients diffusion, cell growth, and tissue regeneration. The aligned and random PVDF nanofibers were fabricated by using different fiber collectors in the process of electrospinning. **Figure 2**a,b show the scanning electron microscopy (SEM) images of the as-prepared nanofibers: the aligned PVDF (a-PVDF) nanofibers are well oriented along the direction of the arrow; in contrast, the random PVDF (r-PVDF) nanofibers have a multi-oriented architecture. The diameter of the PVDF nanofibers was uniform, ranging from 100 to 800 nm and most of them were at the vicinity of 200–300 nm. The elastic moduli of the a-PVDF and r-PVDF were 73.1 and 40.5 MPa, respectively (Figure S2, Supporting Information). In addition, the breaking threshold of a-PVDF nanofibers during stretching is very narrow, which further proves its highly ordered structure. The Fourier transform infrared (FT-IR) spectra show both the α and β phases coexisted in the PVDF nanofibers. The characteristic bands at 532, 613, 762, 870, and 976 cm^{-1} were attributed to the α phase, whereas those at 486, 509, and 839 cm^{-1} were assigned to the β phase (Figure 2c).[9] PVDF has five crystal phases with three chain conformations: *trans–gauche–trans–gauche* conformation (TGTG′) for the α and δ phases, all-*trans* (TTTTT) for β phase, and T3GT3G′ for γ and ε phases.[10] Among them, the β phase has the highest piezoelectricity due to its maximum dipolar moment. To increase the piezoelectric β phase content while keep the morphology intact, the PVDF nanofibers were thermally annealed after the solvent was volatilized. Figure 2d shows the X-ray diffraction (XRD) patterns of the a-PVDF nanofibers after different annealing temperature within the range of 60–140 °C. The diffraction peaks at 20.119° were indexed to the (110) crystal faces of α-phase PVDF (JCPDS No. 42-1650). The diffraction peak located at 20.687° and 20.827° corresponded to (200) and (110) crystal planes of β-phase PVDF (JCPDS No. 42-1649). The intensity ratio of the β-phase peak (I_β) to the α-phase one (I_α) was enhanced from 0.88 to 1.12 for the a-PVDF and from 0.87 to 1.02 for the r-PVDF after annealing from 60 to 140 °C, respectively. The β phase content of PVDF enhanced gradually with the increase of annealing temperature, indicating that thermal annealing can improve the piezoelectricity. Interestingly, the β phase content of a-PVDF was higher than that of the r-PVDF under the same annealing temperature (Figure S3, Supporting Information), which might be due to that the a-PVDF nanofibers were better stretched and polarized during the electrospinning process with a rotating disk as the fiber collector. Piezoresponse force microscopy (PFM) was performed to further verify the piezoelectricity of the PVDF nanofibers. The topographic image (Figure 2e) shows ordered fiber distribution for the a-PVDF nanofibers, in consistent with the SEM data. The phase signal represents the polarization direction underneath the probe tip (Figure 2f). These results proved the piezoelectricity of the a-PVDF. In addition, the hysteresis loops of amplitude at the applied alternating current (AC) voltage from −5 to + 5 V reveal a clear butterfly shape, verifying its piezoelectric properties (Figure 2f). For the a-PVDF, the amplitude reached 9.5 and 5.7 nm under the ±5 V bias. Although with piezoelectricity, the r-PVDF only produced an amplitude of 0.42 and 0.20 nm under the same bias voltage (Figure S5, Supporting Information). According to the quantitative measurement of quasi-static d_{33}, the piezoelectric coefficient d_{33} for the a-PVDF and r-PVDF were 24 and 13 pC N^{-1}, respectively, further indicating the higher piezoelectricity of a-PVDF than r-PVDF.

Rat bone-marrow-derived mesenchymal stem cells (rBMSCs) were seeded on the as-prepared aligned and random PVDF nanofibers to evaluate cell adhesion and proliferation. To improve the hydrophilicity of the scaffolds for cell attachment, the nanofibers were treated with oxygen plasma for 3 min. The water contact angle of the PVDF nanofibers reduced from 123–132° to 52–72° after the plasma treatment (Figure S6,

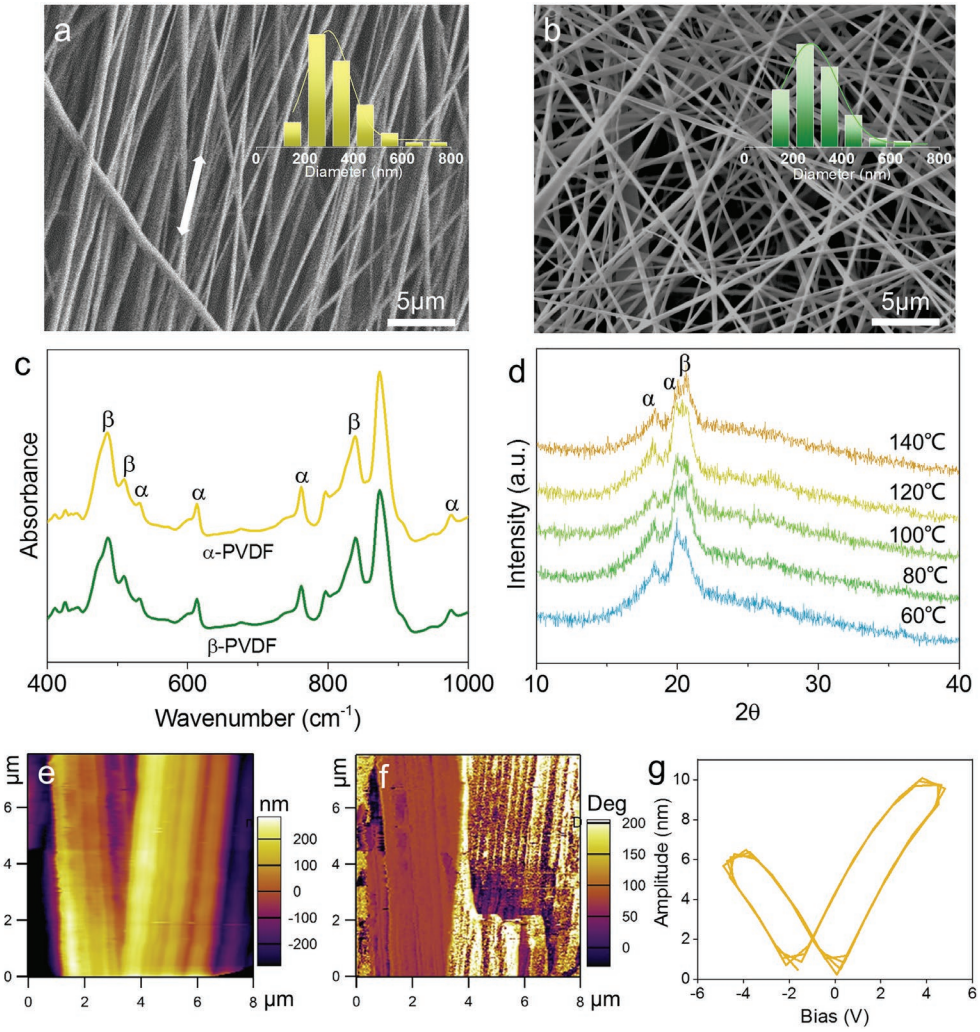

Figure 2. Morphology and piezoelectricity of the PVDF nanofibers. a,b) SEM images of the a-PVDF (a) and r-PVDF (b). c) FT-IR spectra of the PVDF nanofibers. d) XRD spectra of the a-PVDF with different annealing temperature from 60–140 °C. e) AFM topography, f) phase images, and g) amplitude hysteresis loops of the a-PVDF.

Supporting Information). Furthermore, water contact angle of the a-PVDF nanofibers along the fiber extension direction (a-PVDF/p, 123° before plasma treatment and 53° after plasma treatment) was smaller than that along the vertical fiber extension direction (a-PVDF/v, 132° before plasma treatment and 72° after plasma treatment) both before and after oxygen plasma treatment. It was due to the morphological anisotropy and macroscopic ordering of the a-PVDF nanofibers. Live/dead cell staining after 48 h culture of the rBMSCs on the substrates showed that most cells were survived on the nanofibers, and there was no significant difference in cell viability between the PVDF nanofibers and tissue culture plate (TCP) (Figure S8, Supporting Information). From fluorescence microscopy images of F-actin/vinculin/nuclei of rBMSCs after culturing for 48 h, the cells attached and spread well on both the aligned and random PVDF nanofibers (**Figure 3**a). In addition, the cells on the PVDF scaffolds had more protrusions and longer filopodia compared with those on TCP. It was worth noting that the F-actin filaments and nuclei of the cells on the a-PVDF exhibited obvious orientation compared to those on the r-PVDF. From the 2D fast Fourier transform (FFT) image analysis (Figure 3b), two distinct peaks at 90° and 270° indicated that F-actin filaments of the cells on a-PVDF were aligned along the specific direction, which was the nanofibers extension direction seen from the SEM images (Figure S9, Supporting Information). For the cells on the r-PVDF, F-actin filaments were arranged randomly, confirmed by a lack of obvious peaks in the FFT plot. Similarly, the angular histograms showed a narrower cell nuclear angular distribution on the a-PVDF scaffold (Figure 3c), while a wider distribution of cell nuclear angles on the r-PVDF counterpart (Figure 3d). Similarly, cell nuclei preferentially aligned along the direction of the a-PVDF nanofiber extension direction. In contrast, cell nuclei were randomly oriented on the r-PVDF. These results indicated that the scaffold morphology has a significant effect on the orientation of both cell cytoskeleton and nuclei.

FAs are mechanical links between the cells and the extracellular microenvironment. At the adhesion sites, integrins

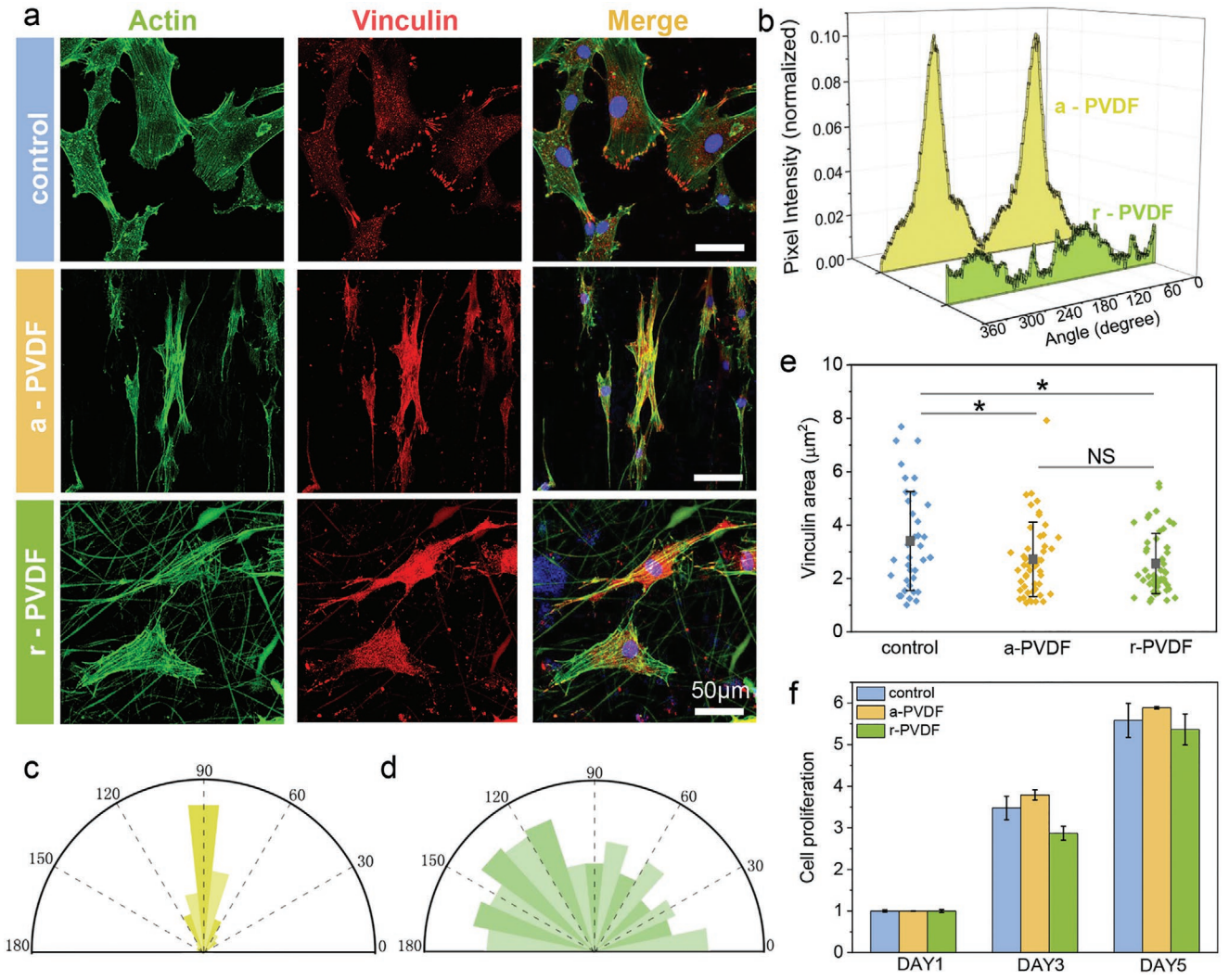

Figure 3. Cytocompatibility and cell attachment. a) Fluorescence microscopy images of the rBMSCs on the TCPs, a-PVDF, and r-PVDF after 48 h culture. F-actin is stained with green, vinculin is stained with red, and nuclei are stained with blue. b) 2D FFT image analysis of F-actin orientation of the cells on the a-PVDF and r-PVDF. c,d) Angular histograms of cell nuclear angles of the a-PVDF (c) and r-PVDF (d). e) Vinculin spot area of rBMSCs on the TCP, a-PVDF, and r-PVDF. f) Histogram of the statistical results of the cell proliferation rate. Error bars, mean ± standard deviation (s.d.) $*p < 0.05$, $**p < 0.01$, NS means no significant difference.

act as the bridge to connect the ECM and intracellular F-actin cytoskeleton and transduce mechanical forces generated by the actin retrograde flow and myosin II to the ECM through mechanosensitive FA proteins.[11] After rBMSCs were seeded on the PVDF nanofibers for 24 h, vinculin was distributed at the tips of the prolonged cell for both PVDF scaffolds and TCP (Figure 3a and Figures S10 and S11, Supporting Information). Nevertheless, rBMSCs on the PVDF nanofibers showed more vinculin positive region at the center of the cells, simultaneously. Generally, punctate structures with micrometer-size indicate the mature FAs.[12] From Figure 3e, rBMSCs on both PVDF scaffolds and TCP had a lot of vinculin structures with area larger than 1 μm^2. Mature FAs are necessary for the adaptive deformation of nanofibers caused by cell traction. Moreover, the FAs of cells on the a-PVDF were highly co-aligned with the cell spreading direction, that is, the extension direction of the nanofibers.

CCK-8 assay was employed to quantify cell proliferation on the PVDF nanofibers. As shown in Figure 3f, the rBMSCs on the PVDF scaffolds had a similar proliferation rate with TCP from the 1st to the 5th day, indicating the good biocompatibility of the PVDF nanofibers. Moreover, there were more cells on the a-PVDF than on the r-PVDF and the TCP on days 3 and 5. It might be due to that the directional spread of the cells on the a-PVDF could reduce the proliferation inhibitory effect caused by cell contact, suggesting that a-PVDF promoted the self-renewal of rBMSCs compared to r-PVDF and TCP. These results demonstrated that rBMSCs on a-PVDF, r-PVDF, and TCPs exhibited different cell morphology, adhesion state, and self-renewal ability.

Electrical stimulation has been developed to mimic the natural bioelectricity as a biophysical cue for modulation of a myriad of biological processes, from cell cycle, migration, proliferation to stem cell differentiation.[13] Considering

the correlation between mechanical–electrical conversion of the piezoelectric fibrous network and the electrical stimulation on the cells, we utilize this cell-traction-triggered on-demand electrical stimulation to regulate stem cell fate. After the cells were cultured for 2 days under normal culture condition to ensure the stem cells adhere well to the nanofibers, the normal culture medium was replaced by neural differentiation medium and cultured for another 7 days to assess the effect of arrangement and piezoelectricity of PVDF nanofibers on neuron-like differentiation of rBMSCs. The differentiated cells on a/r-PVDF, TCPs, and PVDF without further anneal processing (a/r-PVDF (u)) were observed after immunofluorescently stained with the early neural marker β-Tubulin III (Tuj-1), neurogliocyte maker glial fibrillary acidic protein (GFAP), and the later neural marker microtubule-associated protein-2 (MAP-2) (**Figure 4**a and Figure S13, Supporting Information). The expression of both neural and neurogliocyte makers for the cells on PVDF scaffolds were higher than those of TCP and PVDF (u). For the neuronal-specific markers Tuj-1 and MAP-2, there was a significant increase of positive cells on the a-PVDF scaffold, which were about 1.53-fold and 1.38-fold higher than that on the r-PVDF scaffold, respectively. In contrast, there were slightly more GFAP positive cells on the r-PVDF. It is worth noting that the Tuj1-positive cells on the annealed PVDF scaffold were about 2.21-fold (a-PVDF) and 1.87-fold (r-PVDF) higher than those on their unannealed counterparts, respectively (Figure S13, Supporting Information). In addition, the cellular neurites on the a-PVDF extended along the fiber direction with an average length of ≈91 μm, which was much longer than those on the r-PVDF scaffold (≈68 μm, Figure 4c). The cell morphology was further observed via SEM to evaluate neurite sprouting and outgrowth. From Figure 4d,e, the cells after 7 days of differentiation had a spindly morphology possessing thin and elongated protrusions, compared with a flat spreading morphology of rBMSCs after 2 days of adhesion (Figure S12, Supporting Information). These results indicated that the piezoelectric PVDF scaffolds could specifically enhance neuron-like differentiation of rBMSCs, and the a-PVDF was more advantageous.

Comprehensive utilization of physical cues such as substrate topography, stiffness, and electrical stimulation to regulate stem cell fate has great potential in regenerative medicine. In this work, we hypothesized that the nanofiber alignment and piezoelectricity of the a-PVDF were the determinate factors that promoted neural-like differentiation of rBMSCs. Deformation of the piezoelectric scaffolds is a prerequisite for generating and renewing surface piezopotential. In order to directly observe the deformation of the nanofibers caused by cell traction, fluorescent fluorescein isothiocyanate (FITC) was doped into the nanofibers to distinguish them under a fluorescence microscope. After the cells were seeded on the a-PVDF nanofibers for 24 h, the plasma membranes were stained red with DiD Perchlorate (DiIC18(5)) to directly observe the cell location. From the time-lapse confocal imaging, there was obvious cells migration and green nanofibers displacement, indicating that the a-PVDF nanofibers were deformed (Video S2, Supporting Information). Nine points on the nanofibers were randomly selected from the field of view, and their displacement caused by cell traction within 108 min was ranged from 5 to 60 μm (**Figure 5**a,b). To clearly observe the deformation along the nanofibers caused by cell traction, we incorporated fluorescent SiO_2 spheres (FITC-SiO_2) into the nanofibers during electrospinning. Interestingly, the PVDF nanofiber was significantly deformed and crimped in the horizontal direction under cell traction (Figure 5c and Video S3, Supporting Information). In contrast, there was no obvious deformation of the nanofibers after the cells were seeded on a-PVDF nanofibers for only 2 h (generally <1 μm, Video S1, Supporting Information). This difference suggested that the deformation of the nanofibers might be caused by the cell activity after the formation of FAs, whereas the cell spreading process before the formation of FAs on the nanofibers would not sufficiently produce large cell traction force to induce the nanofibers deformation.

To measure the mechanical property of an individual PVDF nanofiber, we performed microscale three-point bending test. A single nanofiber was collected on a 90 μm wide microfabricated Si channel by electrospinning for a short duration (1–3 s). Both ends of the fiber were fixed by depositing platinum (Figure S16, Supporting Information) to meet the assumption of fixed boundary conditions required for the calculation of Young's modulus. Then, the PVDF nanofiber spanning the channels was bent using an atomic force microscopy (AFM) tip with bead (calibrated spring constant of 60.2 pN nm^{-1}) (Figure 5d,e). The force–indentation curve obtained from the bending test of the PVDF nanofiber is shown in Figure 5g, and the Young's modulus can be calculated according to the formula:[14]

$$\mathrm{E} = \frac{l^3}{192I} \times \frac{dF}{dx} \tag{1}$$

in which l is the length of the PVDF nanofiber spanning the channel; I is the moment of inertia and is equal to $1/4\ \pi R^4$ (R is the radius of the nanofiber); and $\mathrm{d}F/\mathrm{d}x$ is the slope of the force–indentation curve obtained from the bending test. Young's modulus of the individual PVDF nanofiber was calculated to be ≈1.12 GPa. It approximated the range of various fibrous biopolymers such as natural piezoelectric collagen (0.5–10 GPa).[14,15] Since cells sense the mechanics of not just a single fiber, but a network composed of many nanofibers, we also measured the stiffness of the a-PVDF nanofiber film (Figure 5f). Representative withdrawal curve measured at the central position of the film is shown in Figure 5h. The Young's modulus was calculated according to the Derjaguin–Muller–Toporov model using the formula:[16]

$$F = \frac{4}{3} E \sqrt{Rd^3} + F_{\mathrm{adh}} \tag{2}$$

in which F is the force acting on the cantilever, F_{adh} is the adhesion force between the probe and the nanofiber film, R is the tip radius, d is the deformation of the nanofiber film, and E is Young's modulus. Young's modulus of the a-PVDF nanofiber film was calculated to be ≈3.4 kPa, which is highly approximate to the rigidity of brain, and tends to regulate neurogenesis.[17]

Transmembrane calcium channel activation and intracellular calcium transients play important roles in regulating stem cell fate.[18] We monitored the intracellular Ca^{2+} concentration over time when the cells were cultured on a-PVDF. There were

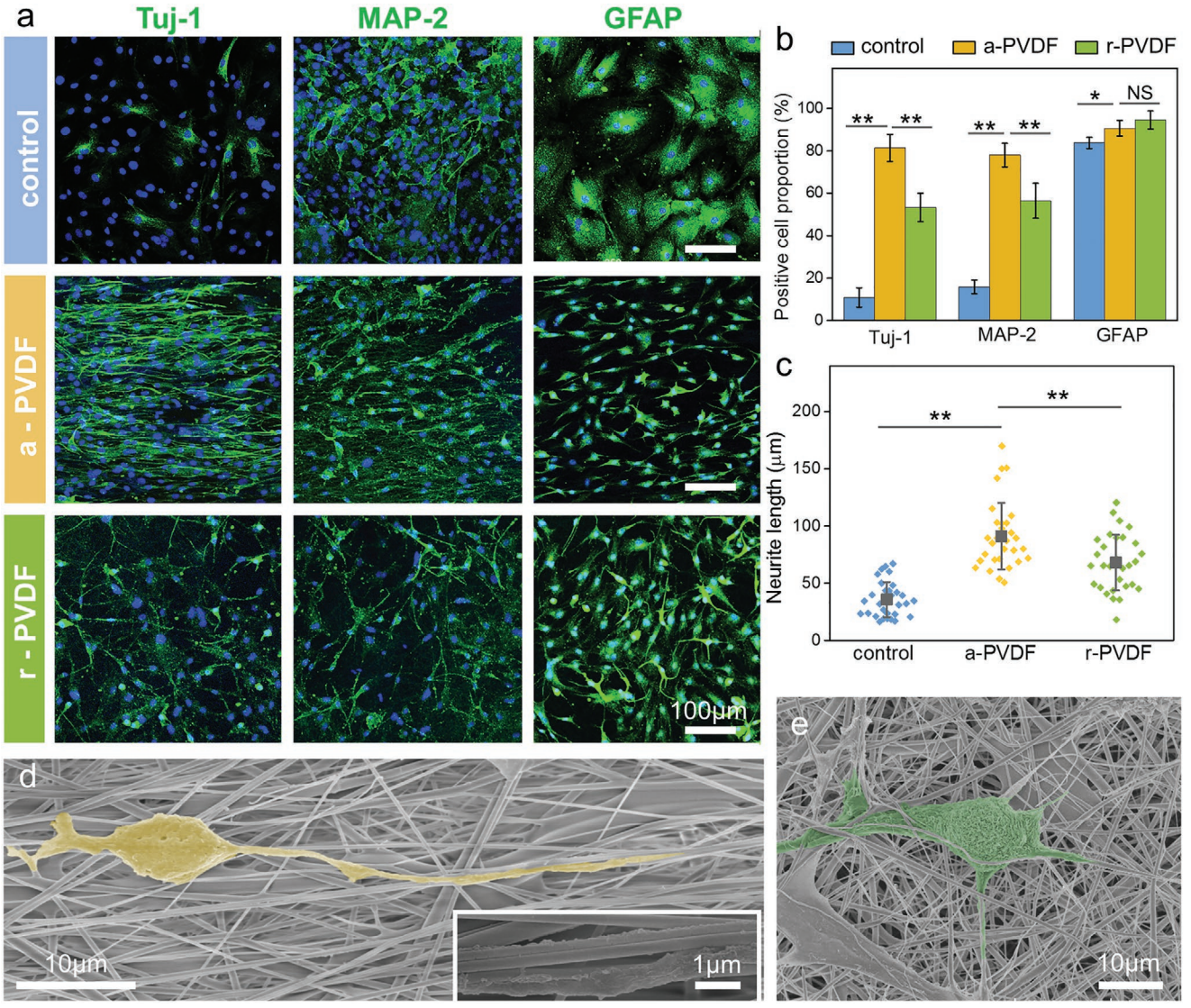

Figure 4. Neuron-like differentiation of rBMSCs on the PVDF nanofibers. a) Immunofluorescent staining of the neuron-specific maker Tuj-1, MAP-2, and a neurogliocyte specific maker GFAP after 7 days of differentiation. The cell nuclei are stained with DAPI (blue), and Tuj-1, MAP-2, and GFAP are immunostained, respectively (green). b) Statistical analysis of the percentage of Tuj-1, MAP-2, and GFAP positive cells. c) Statistical analysis of the neurite length of cells on different samples after 7 days of differentiation. d,e) Representative SEM images of the cells on the a-PVDF (d) and the r-PVDF (e) after 7 days of differentiation. Error bars: mean ± s.d. $*p < 0.05$, $**p < 0.01$, NS means no significant difference.

46.2% (21/39) of the cells on a-PVDF showing obvious transient calcium activity in 1200 s, which was 3.82-fold and 8.56-fold higher than that on the a-PVDF (u) and TCP (**Figure 6**a–c, Figures S17 and S18 and Videos S6–S8, Supporting Information). We speculate that this difference was mainly attributed to the different piezopotential generated by PVDF under cell traction. The cell traction force is typically in the nN range (0.1–10 nN).[19] According to the Young's modulus and piezoelectric coefficient of the nanofibers, the piezopotential caused by cell traction would be from 0.73 to 133 mV. In addition to indirect calculation of the piezopotential caused by the cell traction, we also fabricated a flexible test device to intuitively reflect the generation of piezopotential under an external force. According to Figure 6d and Figure S19, Supporting Information, the output voltage gradually increased from 0.9 to 1.7 V as the external force increased from 0.4 to 1.6 N. Moreover, the output of the a-PVDF nanofibers was higher than that of the r-PVDF under the same external force, which further proved that the a-PVDF nanofibers had a higher piezoelectricity. We also evaluated the piezopotential of a small bundle of nanofibers through their deformation. From Figure 6e and Figure S20, Supporting Information, a small bundle of nanofibers was bridged over a 2 cm wide groove. When the fiber was periodically deformed by 2 mm along the *z*-axis direction, the generated voltage peak was about 0.2 V. The above results indicated that the a-PVDF had an excellent mechanical–electrical conversion performance. Hence, the as-prepared PVDF piezoelectric scaffold allowed sensitive deformation in response to the cellular activities and tractions, thereby generating a significant piezopotential. The generated piezopotential was able to activate the transmembrane

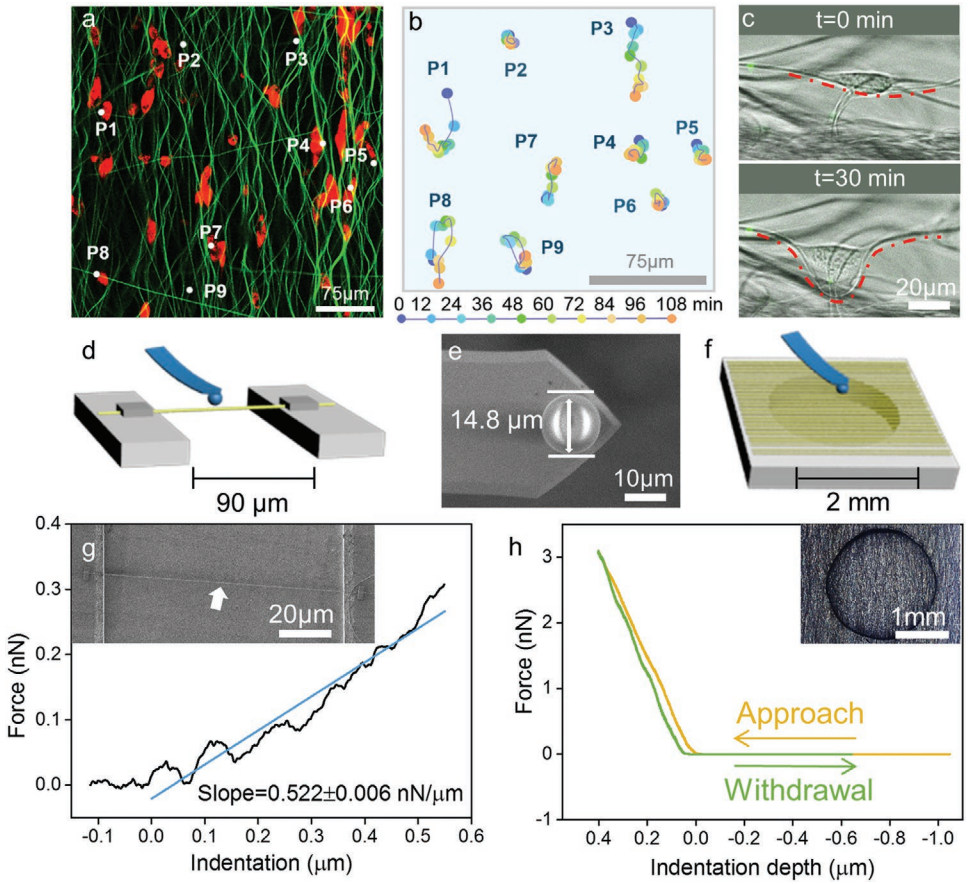

Figure 5. The deformation of the nanofibers caused by cell traction and their mechanical properties. a) Fluorescence image of the PVDF nanofibers (green) and cells (red) after 24 h culture. b) Migration paths of 9 random points of nanofibers within 108 min. c) The deformation along the nanofibers caused by cell traction. The nanofibers are incorporated with FITC-SiO_2 (green). d) Schematic of single fiber three-point bending test performed with AFM. e) SEM image of AFM tip with bead. f) Schematic of stiffness testing of a-PVDF film performed with AFM. g) Force–indentation curve of a PVDF nanofiber. Inset: SEM image of a single nanofiber spanning a channel. h) AFM-based withdrawal force–distance curve of the a-PVDF film. Inset: Image of a-PVDF film on a hollow substrate with a diameter of 2 mm.

calcium channels, allowing an influx of extracellular Ca^{2+} into cytoplasm (Figure 6f). It was worth noting that the deformation of the piezoelectric scaffold was only occurred after cell adhesion, thus realizing the on-demand electrical stimulation in the differentiation stage when needed, and avoiding the inhibitory effect of early electrical stimulation during cell spreading.

3. Conclusion

We have developed a smart piezoelectric scaffold to regulate cell–ECM interaction and feedback to determine stem cell fate in developmental mechanical microenvironments of adherent cells. Importantly, we directly observed the obvious deformation and crimping of the nanofibers caused by cell traction force only after cell adhesion and mature FA formation, which generated about a 98 μV to 18 mV piezopotential to stimulate the stem cells. The rBMSCs on the a-PVDF scaffold differentiated into neuron-like cells when cultured for up to 7 days under this in situ electrostimulation without applying an external mechanical or electrical stimulation. These results help us to reveal the loop feedback between living cells and dynamic ECM, and pave a new way for the design of 4D tissue engineering scaffolds.

4. Experimental Section

Preparation of the PVDF Nanofibers: The aligned and random PVDF nanofibers were prepared by electrospinning. A mixture of dimethylformamide (DMF)/acetone (6:4 by volume) was used as the solvent. The PVDF concentrations of 16, 20, and 24 wt% were prepared by dissolving PVDF tablets (Mw = 27 000, Sigma-Aldrich) in DMF/acetone solvent under a continuous stirring for 6 h at 60 °C. Then, it was collected in a plastic syringe with a 21G steel needle, and a syringe pump was employed to control the flow rate at 1 mL h^{-1}. A fixed voltage of 20 kV was adopted between the syringe needle and the fiber collector with the work distance of 15 cm. For the aligned PVDF nanofibers, a rotating disk with the rotational speed of 1500 rpm was used as the fiber collector, whereas a flat aluminum plat was employed to collect random PVDF nanofibers. Then, the nanofibers were annealed at different temperature for 6 h to increase the crystallinity. To improve hydrophilicity for cell attachment, the nanofibers were treated with oxygen plasma by Plasma Cleaning System (PVA TePla/IoN 40, America) for 3 min. The morphology of the nanofibers was characterized by the field-emission SEM (SU8020, Hitachi). FT-IR spectra were tested by Vertex80V (Bruker Corp., USA) ranging from 400 to 2000 cm^{-1}. XRD patterns were acquired on a

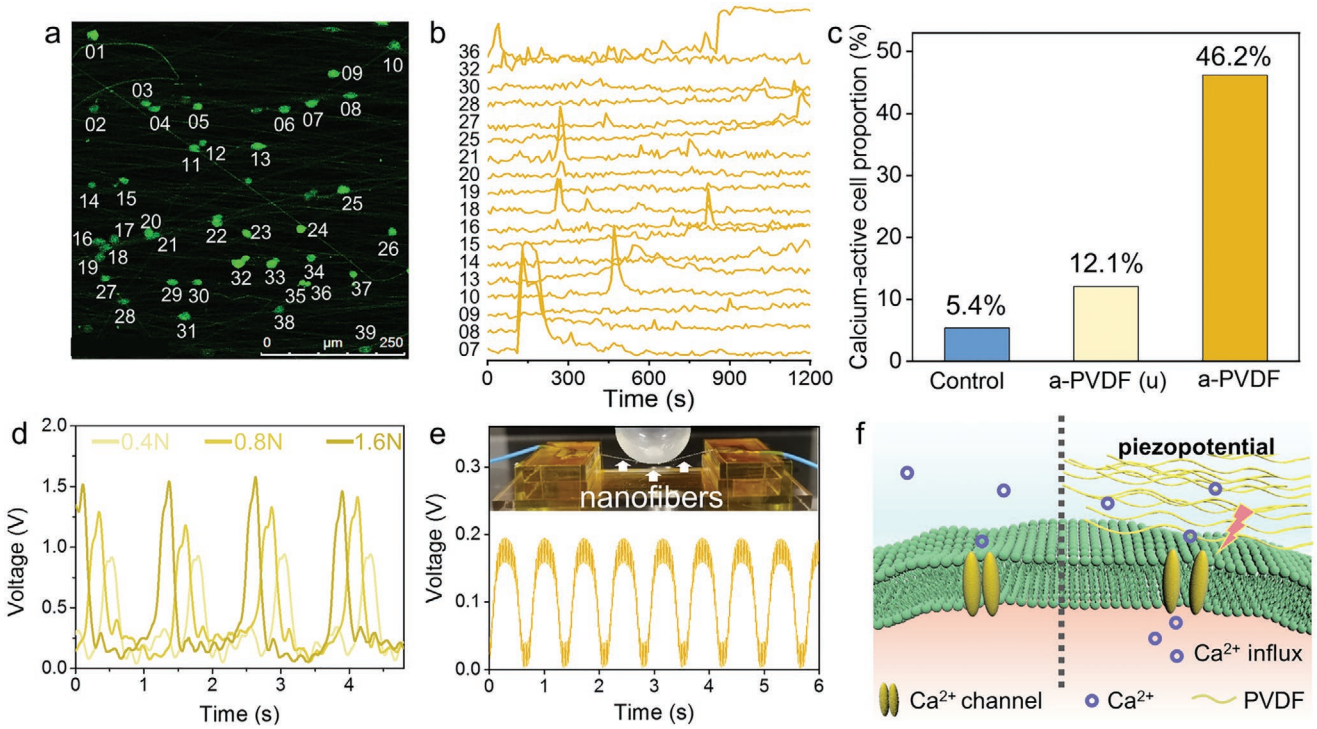

Figure 6. Mechanical–electrical conversion of the piezoelectric PVDF nanofibers and the effect on calcium activity. a) Intracellular calcium staining of rBMSCs on a-PVDF. b) Cells on a-PVDF with obvious transient calcium activity in 1200 s. The numbers represent different cells in the field of view. c) Analyses of calcium-active cells on different samples. d) Output voltage of the a-PVDF under different external forces (0.4–1.6 N). e) Output voltage of a bundle of nanofibers under periodical deformation along the *z*-axis direction. f) Schematic of intracellular calcium transient caused by piezopotential of PVDF. Left: Cells cultured on TCP; Right: Cells cultured on a-PVDF.

Bruker D8 Advance powder XRD with Cu-Kα radiation ($\lambda = 0.15406$ nm). Piezoelectric force microscopy (PFM) measurements were performed at the modulation frequency equipped with external lock-in amplifiers (HF2LI, Zurich Instruments, Switzerland). The water contact angle was acquired by the contact angle measurement (XG-CAMB1, Xuanyi).

Mechanical Testing: To determine the tensile mechanical properties of the PVDF nanofiber films, films were cut into 1 × 3 cm strips and their elastic modulus were measured by a tensile testing machine. Microscale three-point bending test was employed to measure the mechanical property of an individual PVDF nanofiber. A single nanofiber was collected on a 90 µm wide microfabricated Si channel by electrospinning for a short duration (1–3 s). Both ends of the fiber were fixed by depositing platinum to meet the assumption of fixed boundary conditions required for the calculation of Young's modulus. Then, PVDF nanofiber spanning the channels was bent with an AFM tip with a calibrated spring constant of 40.33 pN nm^{-1} positioned centrally along the fiber's length. Young's modulus was calculated from the obtained load–displacement curve using known equations with fixed boundaries. For the piezoelectricity coefficient measurement, the PVDF nanofiber film was sputtered with aluminum electrodes (diameter = 4 mm) on both sides of the surface. And the piezoelectricity coefficient d_{33} was measured using a quasi-static d_{33} measuring instrument (Institute of Acoustics, Chinese Academy of Science, ZJ-4AN, Beijing, China).

Output Voltage Measurement of PVDF: To measure the output voltage of the PVDF nanofiber film, aluminum tapes were pasted on both sides of the film as electrodes. LinMot linear motor (LinMot USA, Inc., Elkhorn, WI, USA) was employed to apply different forces to the film (0.4–1.6 N). The pressure force was monitored by a commercial sensor (501F01, YMC Piezotronics INC) mounted on the motion part of the linear motor. And the generated voltage was measured by Keithley electrometer 6514 (Tektronix Inc., Beaverton, OR, USA).

To test the output voltage of the PVDF nanofibers, a small bundle of nanofibers was picked up by a tweezer and bridged over a 2 cm wide groove. Then, two drops of silver paste were deposited at both ends of the nanofiber tips as electrodes. The fiber was driven by a LinMot linear motor to periodically deform by 2 mm along the *z*-axis direction. The generated voltage was measured by Keithley electrometer 6514.

Cell Culture: rBMSCs were derived from the femurs and tibias of 4 week-old Wistar rats as previously described.[20] The procedures for handling animals strictly followed the Beijing Administration Rule of Laboratory Animals and the national standards of Laboratory Animal Requirements of Environment and Housing Facilities (GB14925-2001). The animal experiments were approved by the Biomedical Ethics Committee of Peking University (Approval Number: LA2018282). rBMSCs were cultured in low-glucose (1.0 g L^{-1}) Dulbecco's modified Eagle medium (L-DMEM, Gibco) containing 10% fetal bovine serum (FBS, Gibco), 1% penicillin–streptomycin (Gibco), and 4 ng mL^{-1} basic fibroblast growth factor (bFGF, Peprotech) under a humidified atmosphere of 5% CO_2 at 37 °C. rBMSCs at the third passage were used for the following experiments.

Neural Differentiation of rBMSCs: To investigate the neural differentiation of rBMSCs on the aligned and random PVDF nanofibers, the cells were seeded on the nanofibers and cultured under normal condition for 48 h, and then the normal culture medium was replaced by neural differentiation medium DMEM/F12 (Gibco) plus 1% FBS, 1% penicillin–streptomycin, 2% B27 supplement (Invitrogen), 20 ng mL^{-1} bFGF (Peprotech), 10 ng mL^{-1} nerve growth factor (NGF, Peprotech), and 10 ng mL^{-1} brain-derived neurotrophic factor (BDNF, Peprotech). The culture medium was changed every two days.

Cell Cytoskeleton and Nuclear Alignment Quantification: A 2D FFT image analysis method was adopted to quantitatively evaluate cell cytoskeleton alignment on the aligned and random PVDF nanofibers.[21] A 1024 × 1024 px image was overlaid with a compatible-sized black square mask with a transparent concentric circle (1024 px in diameter) to avoid the edge effect, and then proceeded with the FFT function in ImageJ. Subsequently, pixel intensity along each angle (from 0° to 359°

with 1° increment) was summed through the plugin "Oval Profile" in ImageJ. The obtained pixel intensity was normalized by dividing the minimum intensity value, and all the normalized pixel intensity was subtracted 1 to shift the baseline to 0.

To quantify the alignment of the cell nuclei, the angle of the cell nuclei was measured using ImageJ.[21a,22] Briefly, the image of nuclei was thresholded using image > adjust > color threshold to make the nuclei more distinguishable. Then, the angle of the cell nuclei was measured by "Particle Analyzer" in ImageJ. Nine images were summed to quantify the degree of cytoskeleton and nuclear alignment for each sample.

Cell Dynamic Observation: A thin a-PVDF scaffold was fabricated by a parallel metal collector in the process of electrospinning, and trace amount of FITC or FITC-SiO_2 was mixed to the spinning solution for better distinguishing the nanofibers when observed using a fluorescence microscope. Then, the a-PVDF nanofibers were transferred to a hollow ring (diameter = 1.5 cm) and placed in a confocal dish. After the cells were seeded on a-PVDF nanofibers for 2 or 24 h, the cells were incubated with DiIC18(5) to stain cytomembrane (4 µM in phosphate buffer saline (PBS)) for 20 min and then washed three times with culture medium to observe the deformation of the nanofibers caused by cell traction using a Leica confocal microscope.

Intracellular Calcium Measurement: The cells were cultured on the samples for 24 h, incubated with 2 µM Fluo-4 AM (Abcam) in PBS for 30 min at room temperature, and further cultured in normal medium for 30 min. The intracellular calcium concentration was measured every 10 s during 1200 s using a Leica confocal microscope.

Statistical Analysis: The data are reported as the means ± s.d., and statistical analysis was performed using the unpaired Student's *t*-test. Statistical significance was accepted at $*p < 0.05$ and $**p < 0.01$.

Supporting Information

Supporting Information is available from the Wiley Online Library or from the author.

Acknowledgements

The work was supported by the National Key R&D project from Minister of Science and Technology, China (2016YFA0202703), the National Nature Science Foundation (No. 82072065, 81471784), the National Youth Talent Support Program, and the China Postdoctoral Science Foundation (Grant No. BX2021299). The authors appreciate the efforts and constructive suggestions from the reviewers to help improve the manuscript.

Conflict of Interest

The authors declare no conflict of interest.

Data Availability Statement

Research data are not shared.

Keywords

dynamic microenvironment, feedback, on-demand electrostimulation, piezoelectric scaffold, stem cell differentiation

Received: August 12, 2021
Revised: September 15, 2021
Published online:

[1] a) Y. Li, Y. Xiao, C. Liu, *Chem. Rev.* **2017**, *117*, 4376; b) N. Mitrousis, A. Fokina, M. S. Shoichet, *Nat. Rev. Mater.* **2018**, *3*, 441.
[2] a) L. Moroni, J. A. Burdick, C. Highley, S. J. Lee, Y. Morimoto, S. Takeuchi, J. J. Yoo, *Nat. Rev. Mater.* **2018**, *3*, 21; b) A. Higuchi, Q.-D. Ling, Y. Chang, S.-T. Hsu, A. Umezawa, *Chem. Rev.* **2013**, *113*, 3297; c) E. S. Place, N. D. Evans, M. M. Stevens, *Nat. Mater.* **2009**, *8*, 457.
[3] a) J. A. Burdick, W. L. Murphy, *Nat. Commun.* **2012**, *3*, 1269; b) J. Kim, R. C. Hayward, *Trends Biotechnol.* **2012**, *30*, 426; c) A. Higuchi, Q. D. Ling, S. S. Kumar, Y. Chang, T. C. Kao, M. A. Munusamy, A. A. Alarfaj, S. T. Hsu, A. Umezawa, *Prog. Polym. Sci.* **2014**, *39*, 1585; d) S. R. Shin, B. Migliori, B. Miccoli, Y. C. Li, P. Mostafalu, J. Seo, S. Mandla, A. Enrico, S. Antona, R. Sabarish, T. Zheng, L. Pirrami, K. Zhang, Y. S. Zhang, K. T. Wan, D. Demarchi, M. R. Dokmeci, A. Khademhosseini, *Adv. Mater.* **2018**, *30*, 1704189; e) L. B. Zhang, Z. J. Wang, J. Das, M. Labib, S. Ahmed, E. H. Sargent, S. O. Kelley, *Angew. Chem., Int. Ed.* **2019**, *58*, 14519.
[4] S. A. Ferreira, M. S. Motwani, P. A. Faull, A. J. Seymour, T. T. L. Yu, M. Enayati, D. K. Taheem, C. Salzlechner, T. Haghighi, E. M. Kania, O. P. Oommen, T. Ahmed, S. Loaiza, K. Parzych, F. Dazzi, O. P. Varghese, F. Festy, A. E. Grigoriadis, H. W. Auner, A. P. Snijders, L. Bozec, E. Gentleman, *Nat. Commun.* **2018**, *9*, 4049.
[5] Z. R. Liu, J. H. Nie, B. Miao, J. D. Li, Y. B. Cui, S. Wang, X. D. Zhang, G. R. Zhao, Y. B. Deng, Y. H. Wu, Z. Li, L. L. Li, Z. L. Wang, *Adv. Mater.* **2019**, *31*, 1807795.
[6] a) K. W. Yong, Y. H. Li, G. Y. Huang, T. J. Lu, W. K. Z. W. Safwani, B. Pingguan-Murphy, F. Xu, *Am. J. Physiol.: Heart Circ. Physiol.* **2015**, *309*, H532; b) B. J. Li, C. Moshfegh, Z. Lin, J. Albuschies, V. Vogel, *Sci. Rep.* **2013**, *3*, 2425; c) S. W. Lane, D. A. Williams, F. M. Watt, *Nat. Biotechnol.* **2014**, *32*, 795; d) K. H. Vining, J. C. Scherba, A. M. Bever, M. R. Alexander, A. D. Celiz, D. J. Mooney, *Adv. Mater.* **2018**, *30*, 1704486.
[7] a) B. M. Baker, B. Trappmann, W. Y. Wang, M. S. Sakar, I. L. Kim, V. B. Shenoy, J. A. Burdick, C. S. Chen, *Nat. Mater.* **2015**, *14*, 1262; b) C. E. Chan, D. J. Odde, *Science* **2008**, *322*, 1687.
[8] R. Ashraf, H. S. Sofi, M. A. Beigh, F. A. Sheikh, *Tissue Cell* **2019**, *59*, 70.
[9] a) Z. Xu, M. Baniasadi, S. Moreno, J. Z. Cai, M. Naraghi, M. Minary-Jolandan, *Polymer* **2016**, *106*, 62; b) D. Dhakras, V. Borkar, S. Ogale, J. Jog, *Nanoscale* **2012**, *4*, 752.
[10] a) H. Yu, T. Huang, M. X. Lu, M. Y. Mao, Q. H. Zhang, H. Z. Wang, *Nanotechnology* **2013**, *24*, 405401; b) H. Shao, J. Fang, H. Wang, C. Lang, T. Lin, *ACS Appl. Mater. Interfaces* **2015**, *7*, 22551.
[11] a) J. Z. Kechagia, J. Ivaska, P. Roca-Cusachs, *Nat. Rev. Mol. Cell Biol.* **2019**, *20*, 457; b) Z. Sun, S. S. Guo, R. Fässler, *J. Cell Biol.* **2016**, *215*, 445; c) B. D. Hoffman, C. Grashoff, M. A. Schwartz, *Nature* **2011**, *475*, 316.
[12] a) C. Turner, *Nat. Cell Biol.* **2000**, *2*, E231; b) Y. Hou, L. Yu, W. Xie, L. C. Camacho, M. Zhang, Z. Chu, Q. Wei, R. Haag, *Nano Lett.* **2020**, *20*, 748.
[13] a) K. Kapat, Q. T. H. Shubhra, M. Zhou, S. Leeuwenburgh, *Adv. Funct. Mater.* **2020**, *30*, 1909045; b) A. J. Petty II, R. L. Keate, B. Jiang, G. A. Ameer, J. Rivnay, *Chem. Mater.* **2020**, *32*, 4095.
[14] L. Yang, K. O. van der Werf, B. F. J. M. Koopman, V. Subramaniam, M. L. Bennink, P. J. Dijkstra, J. Feijen, *J. Biomed. Mater. Res., Part A* **2007**, *82A*, 160.
[15] M. Guthold, W. Liu, E. A. Sparks, L. M. Jawerth, L. Peng, M. Falvo, R. Superfine, R. R. Hantgan, S. T. Lord, *Cell Biochem. Biophys.* **2007**, *49*, 165.
[16] Y. Su, Z. Zhang, Y. Wan, Y. Zhang, M. Chen, *NPG Asia Mater* **2020**, *12*, 55.
[17] a) S. Mitragotri, J. Lahann, *Nat. Mater.* **2009**, *8*, 15; b) X. Y. Wan, Z. R. Liu, L. L. Li, *Adv. Funct. Mater.* **2021**, *31*, 202010626.
[18] Z. R. Liu, X. Y. Wan, Z. L. Wang, L. L. Li, *Adv. Mater.* **2021**, 2007429.
[19] a) A. Ganz, M. Lambert, A. Saez, P. Silberzan, A. Buguin, R. M. Mege, B. Ladoux, *Biol. Cell* **2006**, *98*, 721; b) G. Murillo, A. Blanquer, C. Vargas-Estevez, L. Barrios, E. Ibanez, C. Nogues,

J. Esteve, *Adv. Mater.* **2017**, *29*, 1605048; c) X. D. Zhang, X. Cui, D. C. Wang, S. Wang, Z. R. Liu, G. R. Zhao, Y. Zhang, Z. Li, Z. L. Wang, L. L. Li, *Adv. Funct. Mater.* **2019**, *29*, 1900372.

[20] a) W. B. Guo, X. D. Zhang, X. Yu, S. Wang, J. C. Qiu, W. Tang, L. L. Li, H. Liu, Z. L. Wang, *ACS Nano* **2016**, *10*, 5086; b) D. P. Lennon, J. M. Edmison, A. I. Caplan, *J. Cell. Physiol.* **2001**, *187*, 345.

[21] a) L. F. Tseng, P. T. Mather, J. H. Henderson, *Acta Biomater.* **2013**, *9*, 8790; b) C. E. Ayres, B. S. Jha, H. Meredith, J. R. Bowman, G. L. Bowlin, S. C. Henderson, D. G. Simpson, *J. Biomater. Sci., Polym. Ed.* **2008**, *19*, 603.

[22] P. Davidson, M. Bigerelle, B. Bounichane, M. Giazzon, K. Anselme, *Acta Biomater.* **2010**, *6*, 2590.